

**Dieses Dokument ist eine Zweitveröffentlichung (Verlagsversion) /
This is a self-archiving document (published version):**

Uwe Marschner, Günther Pfeifer, Eric Starke

Reciprocity of linear systems with smart materials utilized for precise measurement techniques

Erstveröffentlichung in / First published in:

Journal of Intelligent Material Systems and Structures. 2016, 27(14), S. 1989 - 2000 [Zugriff am: 12.08.2019]. SAGE journals. ISSN 1530-8138.

DOI: <https://doi.org/10.1177/1045389X16642531>

Diese Version ist verfügbar / This version is available on:


<https://nbn-resolving.org/urn:nbn:de:bsz:14-qucosa2-356253>

„Dieser Beitrag ist mit Zustimmung des Rechteinhabers aufgrund einer (DFGgeförderten) Allianz- bzw. Nationallizenz frei zugänglich.“

This publication is openly accessible with the permission of the copyright owner. The permission is granted within a nationwide license, supported by the German Research Foundation (abbr. in German DFG).

www.nationallizenzen.de/

Reciprocity of linear systems with smart materials utilized for precise measurement techniques

Journal of Intelligent Material Systems and Structures
2016, Vol. 27(14) 1989–2000
© The Author(s) 2016
Reprints and permissions:
sagepub.co.uk/journalsPermissions.nav
DOI: 10.1177/1045389X16642531
jim.sagepub.com


Uwe Marschner¹, Günther Pfeifer¹ and Eric Starke²

Abstract

In electromechanical measurement techniques, passive transducers and passive electrical networks often interact. In some applications, continua are considered as part of the system, where fields are formed and waves are propagated. In this article, networks, continua, and electromechanical transducers feature sufficient amplitude linear behavior in their environment (e.g. for operation around a bias) and are reciprocal. In addition, all elements of the system have constant parameters during the measurement. Then, the skillful application of the inherent reciprocity of these systems can lead to surprisingly useful benefits. This is shown by actual examples from metrology. The examples include the precise determination of transduction coefficients. It is also shown how the linearity of a system is checked by utilizing reciprocity relations. Although the facts of the matter are well known, its potential is often overlooked or disregarded in measurement techniques.

Keywords

piezoelectric, actuator, sensor, reciprocity, piezomagnetic

Introduction

The description of time-invariant systems with negligible nonlinearity by linear networks is not limited to a single physical domain. In particular, electromechanical and electroacoustic systems of different actuatoric and sensory applications can be described graphically with linear networks in the form of a circuit representation. The heart of such sensors and actuators are often reciprocal transducers (Gerlach and Dötzel, 2008; Lenk et al., 2010). Such a concise system representation not only supports the understanding of the physical operation of systems in design and analysis but also supports the application of the linear network theory allowing significant circuit simplifications in order to expose the dynamic system core. The circuit description is also essential for an efficient simulation of the dynamic system behavior using powerful circuit simulators.

In addition, linear time-invariant and reciprocal—sometimes denoted as reversible—networks possess properties that form the basis for accurate measuring methods. For example, this way acoustic fields can be treated in an analytically elegant manner with the help of reciprocal relations. In this article, the reciprocity in such networks is justified at the beginning of the article by the example of an electromechanical transducer.

The transducer can include, for example, piezoelectric or piezomagnetic materials, which are discussed in detail next. This is followed by two examples of the current applications of reciprocity. One application is the calibration of acceleration sensors. Its specialty is that a mechanical quantity is determined based only on electrical measurements, which can be carried out very precisely. The other application deals with the primary calibration of laboratory standard microphones. Lower measurement uncertainties cannot be currently obtained with any other method. The method does not depend on the applied material. Furthermore, in the last section of the article in addition a method is outlined, where smallest nonlinearities can be examined based on reciprocal measurements.

¹Institute of Semiconductors and Microsystems, Technische Universität Dresden, Dresden, Germany

²Institute of Lightweight Engineering and Polymer Technology, Technische Universität Dresden, Dresden, Germany

Corresponding author:

Uwe Marschner, Institute of Semiconductors and Microsystems, Technische Universität Dresden, 01062 Dresden, Germany.
Email: uwe.marschner@tu-dresden.de

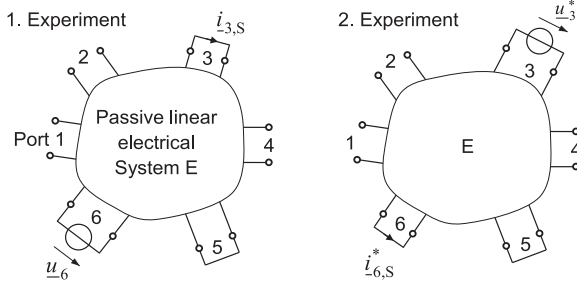


Figure 1. Reciprocal experiments at an electrical system.

Reciprocity in linear networks with reciprocal transducers

In an electrical network, the electrical voltage serves as across quantity and the electrical current as through quantity at an electrical port or terminal, respectively. See, for example, Reibiger (2011) for a general introduction to network theory. For any electrical n -port, which consists of interconnected reciprocal subnetworks (e.g. resistors, capacitors, inductors, and transformers) and space-limited continua (where all linear processes are admissible), it can be shown that it is reciprocal (Desoer and Kuh, 1969; Koenig et al., 1967; Kuh and Rohrer, 1967; Reinschke and Schwarz, 1976).

The reciprocity property can be checked by hand of two sample experiments. Given the system E in Figure 1 with six ports, two ports are selected first. In Figure 1, these are ports 3 and 6; the remaining ports can be open- or short-circuited. These boundary conditions have to be retained in both experiments. In the first experiment, a sinusoidal voltage with the complex magnitude, expressed by the underline, $\underline{u}_6 = \hat{u}_6 e^{j\varphi_{u_6}}$ is applied at port 6 and the steady-state short-circuit current $\underline{i}_{3,S}$ is measured at port 3. In the second experiment, the excitation and measurement ports are reversed, that is, $\underline{i}_{6,S}^*$ is measured while \underline{u}_3^* is applied. It turns out that equation (1) applies for the linkage of the two pairs of through and across quantities

$$\frac{\underline{i}_{3,S}}{\underline{u}_6} = \frac{\underline{i}_{6,S}^*}{\underline{u}_3^*} \quad (1)$$

This law indicates the reciprocity of a passive linear network. It is not limited to electrical systems but also applies to systems incorporating various physical structures.

Analogous to the electrical system E, the experiments can be performed on a passive electromechanical system with reciprocal transducers to detect reciprocity relations. As stated for electrical systems, the electromechanical system consists of interconnected reciprocal subnetworks. Besides the electrical elements, these are, for example, compliances, masses, reluctances, acoustical masses, and acoustical compliances, as well as space-limited continua. The across and through

Table 1. Port (terminal) quantities of different physical systems.

	Across quantity	Through quantity
Electrical system	Voltage, u	Electrical current, i
Mechanical system	Velocity, v	Force, F
Acoustic system	Pressure, p	Volume flow, q

quantities in different physical subsystems in this article are listed in Table 1. Reciprocal transducers relate consistently pairs of through and across quantities of different physical structures to each other (Lenk et al., 2010). These, so-called “passive,” transducers between two ports do not include internal energy sources, that is, the total delivered power at one port is provided by the other port.

With regard to an arbitrary passive linear electromechanical system, reciprocal experiments can cover arbitrary electrical and mechanical ports, as emphasized by Marschner et al. (2013). In the first experiment, for two selected ports, a voltage \underline{u}_n is applied and the blocked force $\underline{F}_{i,S}$ measured. In the second experiment, excitation port and measurement port are exchanged, that is, the short-circuit current $\underline{i}_{n,S}^*$ measured while the velocity \underline{v}_i^* is applied. The other ports may remain open- or short-circuited (or mechanically blocked), but these boundary conditions have to be kept during both experiments. The two experiments result in the equality of the two ratios

$$\frac{\underline{F}_{i,S}}{\underline{u}_n} = \pm \frac{\underline{F}_{n,S}^*}{\underline{v}_i^*} \quad (2)$$

For electromechanical transducers, further reciprocity relations can be derived as a subset of all the transfer functions

$$\frac{\underline{v}_O}{\underline{i}} = \pm \frac{\underline{u}_O^*}{\underline{F}^*} \quad (3)$$

$$\frac{\underline{v}_O}{\underline{u}} = \pm \frac{\underline{i}_S^*}{\underline{F}^*} \quad (4)$$

$$\frac{\underline{F}_S}{\underline{i}} = \pm \frac{\underline{u}_O^*}{\underline{v}^*} \quad (5)$$

where the plus sign is related to magnetic transducers and the minus sign to electric transducers. The linked pairs of flow and differential quantities are marked in Figure 2. The indices S and O denote short circuit and open circuit, respectively. In the transducer, only reciprocal processes are allowed in accordance with thermodynamics. For such transducers, the separation of losses into the surrounding network out of the transducer succeeds. Electrical and magnetic transducers fulfill this condition (Lenk et al., 2010).

In metrology, the calibration of accelerometers is a classic application of the reciprocity relations. A

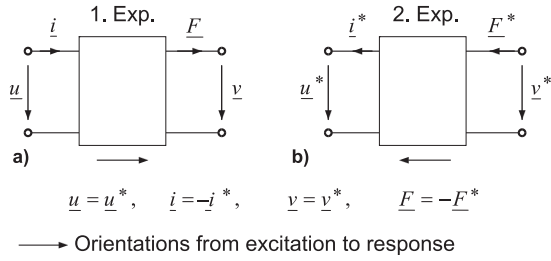


Figure 2. Reference arrow directions of electromechanical transducers for (a) electrical excitation and (b) mechanical excitation.

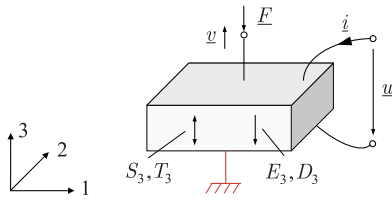


Figure 3. Free piezoelectric thickness oscillator (Lenk et al., 2010).

mechanical calibration source is not required, but any arbitrary additional electromagnetic transducer can be used. This application is analyzed in the second part of the article.

The application of reciprocity relations furthermore proves to be advantageous when continua are part of the system. In 1926, Schottky applied the reciprocity theorems of classical vibration theory for the determination of reception and transmission properties of electroacoustic transducers. Thus, the effect of an impacting quasi-spherical wave on a surface element could be calculated from their emission efficiency. Schottky illustrates the methodology on the example of an electrodynamic horn speaker which prefers low frequencies when it is used as receiver. The law led to the mathematical theory of the receiving cone. The actuality of the methodology is demonstrated by an electroacoustic example.

In the last part of the article the linearity of an electromechanical system is checked by hand of reciprocity relations, where in addition the excitation signal magnitudes are increased. When the related experiments approve the reciprocity, the system behaves linearly. When the reciprocity relations are violated, the system behaves non-linearly. A simple model is applied to describe the source of nonlinearity.

Reciprocity of piezoelectric transducers

Reciprocity of piezoelectric materials is explicitly included in their field equations

$$D_n = \sum_{m=1}^3 \varepsilon_{nm}^T E_m + \sum_{j=1}^6 d_{nj} T_j, \quad n = 1, \dots, 3$$

$$S_i = \sum_{m=1}^3 d_{mi}^* E_m + \sum_{j=1}^6 s_{ij}^E T_j, \quad i = 1, \dots, 6 \quad (6)$$

where D is the electric displacement, ε the permittivity, E the electric field strength, T the mechanical stress, S the mechanical strain, and s the elastic compliance. The piezoelectric coefficients $d_{xy} = d_{xy}^*$ are equal near the operating point. The superscript T denotes that this ε can be measured for $T = 0$. The superscript E denotes the boundary condition $E = 0$, where s can be measured.

Application of boundary conditions and integration gives a device description. It is shown below how the reciprocity of the constitutive field equations is transferred to the device equations. In case of a free thickness oscillator, for example, see Figure 3, only the fields in direction 3 are non-zero

$$E_3, D_3 \neq 0$$

$$E_1, E_2, D_2, D_1 = 0$$

$$T_3 \neq 0$$

$$T_1, T_2, T_4, \dots, T_6 = 0 \quad (7)$$

and equation (6) reduces to

$$D_3 = \varepsilon_{33}^T E_3 + d_{33} T_3$$

$$S_3 = d_{33} E_3 + s_{33}^E T_3 \quad (8)$$

or, with the elastic coefficient c and the piezoelectric modulus e to

$$T_3 = \underbrace{\frac{1}{s_{33}^E}}_c S_3 - \underbrace{\frac{d_{33}}{s_{33}^E}}_e E_3$$

$$D_3 = \underbrace{\varepsilon_{33}^T \left(1 - \frac{d_{33}^2}{\varepsilon_{33}^T s_{33}^E}\right)}_e E_3 + \underbrace{\left(\frac{d_{33}}{s_{33}^E}\right)}_e S_3 \quad (9)$$

Integration of uniform fields and transitions to complex quantities gives voltage $\underline{u} = l_{el} \underline{E}$, current $\underline{i} = j\omega A_{el} \underline{D}$, force $\underline{F} = -A_{mech} \underline{T}$, and velocity $\underline{v} = j\omega l_{mech} \underline{S}$. From equation (9) follows

$$\underline{i} = j\omega \varepsilon \underbrace{\frac{A_{el}}{l_{el}}}_{C_b} \underline{u} + \underbrace{\frac{A_{el}}{l_{mech}}}_{1/Y} e \underline{v}$$

$$\underline{F} = e \underbrace{\frac{A_{mech}}{l_{el}}}_{1/Y} \underline{u} - \underbrace{\frac{1}{j\omega \frac{l_{mech}}{c A_{mech}}}}_{n_s} \underline{v} \quad (10)$$

Circuit interpretation of equation (10) leads to the well-known circuit in Figure 4 (Lenk et al., 2010).

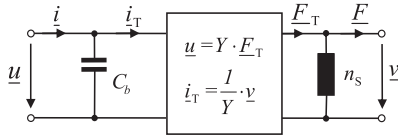


Figure 4. Equivalent circuit of a piezoelectric transducer.

For free thickness oscillators, the network parameters can be analytically determined: the transduction coefficient

$$Y = \frac{l_{\text{mech}} s_{33}^E}{A_{\text{el}} d_{33}} \quad (11)$$

with the thickness l_{mech} working in actuation and sensing direction, respectively, area A_{el} of the piezo block and electrodes, the piezoelectric constant d_{33} , the elastic constant s_{33}^E , as well as the short-circuit compliance

$$n_s = s_{33}^E \frac{l_{\text{mech}}}{A_{\text{mech}}} \quad (12)$$

and the mechanically blocked capacitance

$$C_b = \varepsilon \frac{A_{\text{el}}}{l_{\text{el}}} = C_f - \frac{n_s}{Y^2} \quad (13)$$

with permittivity ε . The mechanically free capacitance C_f differs from C_b by the transformed compliance. The boundary condition-dependent network parameters for other oscillator types can be found, for example, in Lenk et al. (2010).

The reciprocity of this transducer *device* or two-port is checked exemplarily by means of equations (2) and (3). To verify equation (2), the transducer in Figure 4 is excited with a voltage source and a velocity source subsequently. These difference quantities act directly at the transformer core. All flow quantities of the transducer core are directly accessible if the related other physical domain is short-circuited or blocked, respectively. The first reciprocity relationship can thus be read from the transducer core equations

$$\frac{F_s}{u} = -\frac{i_s^*}{v^*} = \frac{1}{Y} \quad (14)$$

The negative sign is due to the reversed direction of the short-circuit current compared to the defined direction of i_w .

To prove the reciprocity relation (3), a current i is supplied in the transducer in the first experiment. With this excitation, the idle velocity v_o of the freely vibrating port is measured. In the second experiment, a force F^* is applied to the mechanical gate and the open-circuit voltage u_o^* is measured. To calculate the transfer functions, the transducer is eliminated by transformation of the transducer components into the other physical domain as shown in Figure 5.

Considering the first experiment, the electrical side of the transducer results in the relationship

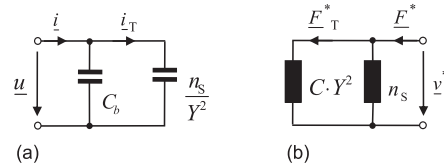


Figure 5. Transformation of piezoelectric transducer components in Figure 4 to prove reciprocity equation (3). (a) Transformation of the short-circuit compliance and (b) transformation of the blocked capacitance.

$$\frac{v_o}{i} = Y \frac{i_T}{i} = Y \frac{\frac{1}{j\omega C_b}}{\frac{1}{j\omega C_b} + \frac{Y^2}{j\omega n_s}} = Y \frac{1}{1 + \frac{C_b Y^2}{n_s}} \quad (15)$$

and, considering the second experiment, at the mechanical side with $u = Y \cdot F = -Y \cdot F^*$ in the relation

$$\frac{u_o^*}{F^*} = -Y \frac{F_T^*}{F^*} = -Y \frac{j\omega n}{j\omega C_b Y^2 + j\omega n} = -Y \frac{1}{1 + \frac{C_b Y^2}{n_s}} \quad (16)$$

From equations (15) and (16) follows equation (3) for electric transducers

$$\frac{v_o}{i} = \frac{u_o^*}{F^*} \quad (17)$$

The other reciprocity relationships can be checked similarly.

Reciprocity of piezomagnetic transducers

One-dimensional magnetomechanical transducer

When a magnetostrictive rod resides as solenoid core freely (stresses $T_1, T_2, T_4, \dots, T_6 = 0$) at the transducers center, as investigated by Kellogg et al. (2005), a one-dimensional (1D) translational transducer model—similar to the piezoelectric transducer—can be derived. Considering the field quantities stress T and magnetic field strength H to be independent variables, the total differentials

$$B_n = \sum_{m=1}^3 \mu_{nm}^T H_m + \sum_{j=1}^6 d_{nj} T_j, \quad n = 1, \dots, 3 \quad (18)$$

$$S_i = \sum_{m=1}^3 d_{mi}^* H_m + \sum_{j=1}^6 s_{ij}^H T_j, \quad i = 1, \dots, 6$$

give the linear constitutive equations for flux density B and strain S in a piezomagnetic body at an operating point. When H is applied in parallel to T , then equation (18) yields for complex quantities

$$\underline{B}_3 = \mu_{33}^T \underline{H}_3 + d_{33} \underline{T}_3 \quad (19)$$

$$\underline{S}_3 = d_{33}^* \underline{H}_3 + s_{33}^H \underline{T}_3$$

with permeability μ_{33}^T (measurable for $T = 0$), piezo-magnetic transduction coefficient d_{33} , and Young's modulus $1/s_{33}^H$ (measurable for $H = 0$). Assuming uniform fields, the simplified relations $B = \Phi/A$, $H = V_m/l$, $T = F/A$, and $S = \xi/l$ with the geometrical parameters length l and area A result. The equations relate B to the magnetic flux Φ , H to the magnetic voltage (or magnetomotive force) V_m , T to force F , and S to displacement ξ and velocity v , respectively. Then equation (19) yields to (Marschner, 2008)

$$\begin{aligned} \underline{\Phi} &= \frac{1}{\mathcal{R}_{m,f}} \underline{V}_m + d_{33} \underline{F} \\ \frac{v}{j\omega} &= d_{33} \underline{V}_m + n_k \underline{F} \end{aligned} \quad (20)$$

in the complex domain. Equation (20) includes the body properties' compliance $n_s = s_{33}^H \cdot l/A$, which can be measured when the magnetic voltage resides at its operating point, that is, here $\underline{V}_m = 0$, and magnetic reluctance $R_m = l/(\mu_{33}^T A)$, measurable for $\underline{F} = 0$. In order to be consistent with network elements and to obtain real transducer factors, the magnetic flux is differentiated to flux rate $\underline{L}_m = j\omega \underline{\Phi}$. Using this quantity and setting the translational transduction coefficient of the piezomagnetic gyrator to $Y_t = n_s/d_{33}$ and $\underline{F}^- = -\underline{F}$, to assure the defined network orientation, from equation (20) follows

$$\begin{aligned} \underline{L}_m &= j\omega \left(\underbrace{\frac{1}{\mathcal{R}_{m,f}} - \frac{d_{33}^2}{n_s}}_{1/\mathcal{R}_{m,b}} \underline{V}_m + \underbrace{\frac{d_{33}}{n_s}}_{1/Y_m} v \right) \\ \underline{F}^- &= \frac{d_{33}}{n_s} \underline{V}_m - \frac{1}{j\omega n_s} v \end{aligned} \quad (21)$$

Equation (21) characterizes a piezomagnetic transducer in the mechanical domain by its compliance n_s and in the magnetic domain by its magnetic reluctance $\mathcal{R}_{m,f}$, which is decreased by $d_{33}^2/n_s = Y_t^2 n_s$ to $\mathcal{R}_{m,b}$, as shown in Figure 6. The core relations of this magnetomechanical transducer have gyratoric character.

1D electromechanical transducer utilizing a solenoid

A long and thin solenoid coil (radius $r \ll l$) can be seen as ideal electromagnetic transducer with transduction coefficient N , acting between magnetic flux rate to voltage u and electrical current i to magnetic voltage when Faraday's law, $\underline{u} = j\omega AN \underline{B}$, and Ampere's law, $\underline{H} = N/\underline{l}$, are applied (Carpenter, 1968; Deskur, 1999). Figure 7 shows the coupling of the piezomagnetic transducer with the electromagnetic solenoid transducer. The circuit can be simplified. First, the reluctance is transformed into the electrical domain, where it appears as inductance $L = \mu A/lN^2$. In the next circuit, the transducers can be combined to one electromechanical transducer with transduction coefficient X as

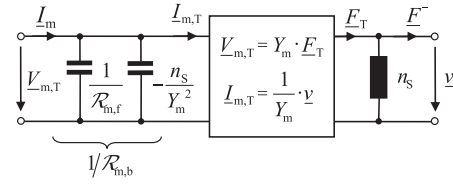


Figure 6. Translational magnetomechanical two-port model of a piezomagnetic transducer.

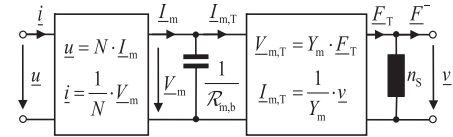


Figure 7. Model of a piezomagnetic transducer residing as solenoid core.

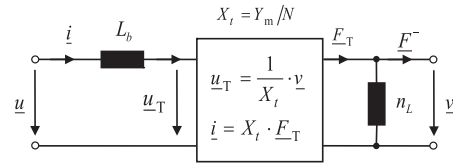


Figure 8. Electromechanical model of a piezomagnetic transducer after reluctance transformation into L_b and transducer combination in Figure 7.

shown in Figure 8. Compared to the piezoelectric transducer, the solenoid with piezomagnetic core exhibits transformer properties. This explains the plus sign in reciprocity relations (2)–(5).

Equation (5) can be easily checked. In order to resolve this equation, an electrical current is applied to the electrical port. The current is transformed into \underline{F}_T , which is equal to the blocked force \underline{F}_S . It follows that

$$\frac{\underline{F}_S}{i} = \frac{1}{X_t} \quad (22)$$

In a second experiment, a velocity source v^* is exciting the system. In case of an open electrical port ($i = 0$), the measurable voltage u_O^* is equal to the internal voltage u_T . The experiment results in

$$\frac{u_O^*}{v^*} = \frac{1}{X_t} = \frac{\underline{F}_S}{i} \quad (23)$$

The other reciprocity relations can be proved similarly by application of the network theory.

Piezomagnetic unimorph

Two-layer piezomagnetic elements with a magnetic and a non-magnetic layer are being used in bending actuators or sensors. In contrast to volume transducers, two-layer elements achieve significantly larger

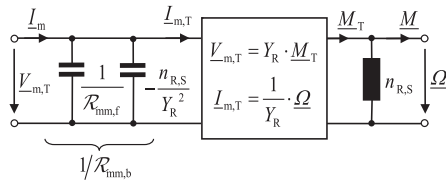


Figure 9. Piezomagnetic unimorph core in a solenoid.

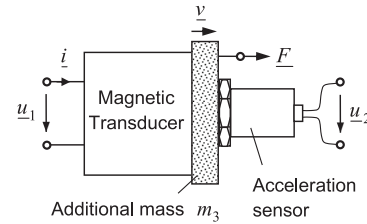


Figure 11. Acceleration sensor calibration setup.

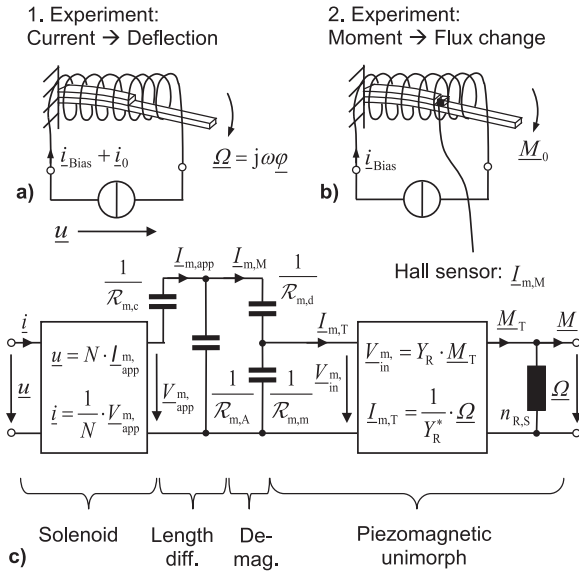


Figure 10. (a) and (b) Performed reciprocal experiments. (c) Rotational electromechanical model of a piezomagnetic unimorph core in a solenoid, as derived in Marschner et al. (2014a). The length difference between coil and magnetostrictive patch constitutes a magnetic voltage divider ($\mathcal{R}_{m,c} + \mathcal{R}_{m,A}$) and demagnetization effects a second magnetic voltage divider ($\mathcal{R}_{m,d} + \mathcal{R}_{m,m}$).

displacements. The dynamic magnetomechanical behavior of such a unimorph can be described by the equivalent circuit in Figure 9, as it is derived by Marschner et al. (2014b). The transduction coefficient Y_R relates bending moment \underline{M}_T and magnetic voltage to each other, as well as rotational velocity $\underline{\Omega}$ and magnetic flux rate \underline{I}_m . The parameter $n_{R,S}$ aggregates the bending compliance and the parameter $\mathcal{R}_{mm,f}$ the mechanical free reluctance similar to the piezomagnetic translational 1D transducer. This reluctance is reduced to $\mathcal{R}_{mm,b}$ in the mechanically blocked case ($\underline{\Omega} = 0$).

In Marschner et al. (2014a), the reciprocal transducer properties of a piezomagnetic unimorph were investigated. The unimorph with the reluctance $\mathcal{R}_{mm,b} = \mathcal{R}_{m,m}$ in Figure 10(c) took up only a section of the surrounding solenoid coil. The tip displacement due to induced strain actuation in a unimorph cantilever beam as well as the sensing response from the patch for bending moments acting on the unimorph were

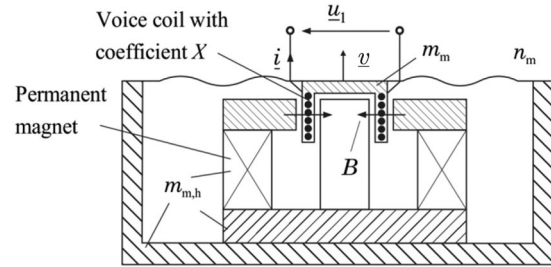


Figure 12. Magnetic transducer setup.

independently measured by S. Datta, as shown in Figure 10(a) and (b). The determined transduction coefficients Y_R and Y_R^* for actuation and sensing were nearly equal and thus capture the reciprocity and linearity of the investigated transducers.

Application of the reciprocity relationship for the calibration of acceleration sensors

A classic application of the reciprocity relations is the calibration of accelerometers. The calibration requires no mechanical calibration source, but an arbitrary additional electromagnetic transducer as depicted in Figure 11. Both transducers, the magnetic transducer and the accelerometer, are connected via mass m_3 .

The construction of the standard magnetic transducer is depicted in Figure 12. Two masses are involved: the mass of all components, which move with the housing $m_{m,h}$, and the total mass of all components, which move with the vibration table m_m . From this magnetic transducer, the mechanical input impedance $\underline{z}_L = (\underline{F}/\underline{v})_{i=0}$ for the electrical open connector must be known.

A piezoelectric accelerometer is mounted exemplarily to the vibration table. Piezoelectric accelerometers contain a piezoelectric ceramic as electromechanical transducer element. This ceramic can be used in the form of a circular-shaped element (for thickness oscillators) or a rectangular element (for bending and shear oscillators). The basic structure of an accelerometer with circular-shaped element is shown in Figure 13. Upon application of forces in the drawn direction, an electrical voltage is generated between the metallized

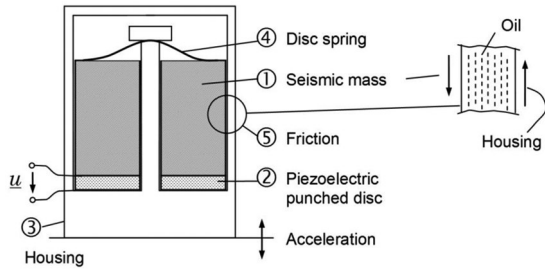


Figure 13. Piezoelectric acceleration sensor construction.

electrodes. The magnitude of the no-load voltage $u_{2,0}$ depends on the characteristics of the piezoelectric ceramic used, on the thickness h of the element, and the surface A on which the force acts.

The equivalent circuit of the mechanical components of the accelerometer in Figure 14 shows the compliances of the disk spring and the piezoelectric ceramic, which act in parallel. The equivalent circuit shows that the sensor exhibits bandpass properties. Low-frequency accelerations do not have an effect on the seismic mass.

The completed equivalent circuit of the calibration system is depicted in Figure 15. All masses establish a virtual connection to the inertial frame. The mass of the sensor is considered to be a part of the transducer system. Thus, impedance z_L must be measured with the attached sensor. The sensor reacts to an acceleration a with the voltage u_2 :

$$u_2 = \underline{B}_a a = j\omega \underline{B}_a v \tag{24}$$

It is the goal of the calibration to determine the transfer function \underline{B}_a .

The calibration utilizes the electromechanical reciprocity relation of the magnetic transducer

$$\frac{v_0}{i_1} = \frac{u_{1,0}}{F} = \underline{B}_R \tag{25}$$

Calibration requires two experiments, as shown schematically in Figure 16. First, an electric current i is fed into the auxiliary magnetic transducer and the open-circuit voltage $u_{2,1}$ is measured. From this measurement, the impedance can be determined. The impedance can be expressed with relations (24) and (25) by

$$\frac{u_{2,0}}{i_1} = j\omega \underline{B}_a \underline{B}_R \tag{26}$$

In the second experiment, an external force F^* stimulates the system that reacts with the open-circuit voltages $u_{1,0}^*$ and $u_{2,0}^*$ at both electrical ports, which are measured and divided by each other

$$\begin{aligned} u_{1,0}^* &= \underline{B}_R F^* \\ u_{2,0}^* &= j\omega \underline{B}_a v^* \\ \frac{u_{1,0}^*}{u_{2,0}^*} &= \frac{\underline{B}_R}{j\omega \underline{B}_a} \frac{F^*}{v^*} = \frac{\underline{B}_R}{j\omega \underline{B}_a} z_L \end{aligned} \tag{27}$$

Typically, the calibration system is designed in a way that good approximation of $z_L = j\omega m_{tot}$ can be

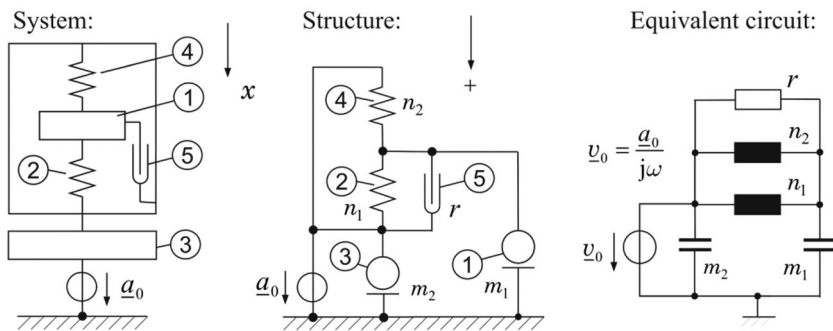


Figure 14. Mechanical part of a piezoelectric acceleration sensor, its structure, and circuit description; the force on n_1 determines the transduced voltage.

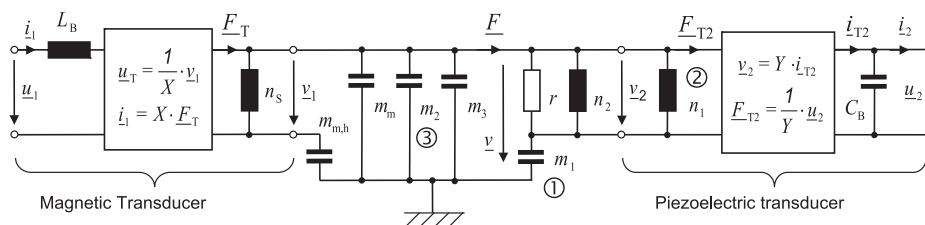


Figure 15. Equivalent circuit of the piezoelectric transducer calibration setup in Figure 11.

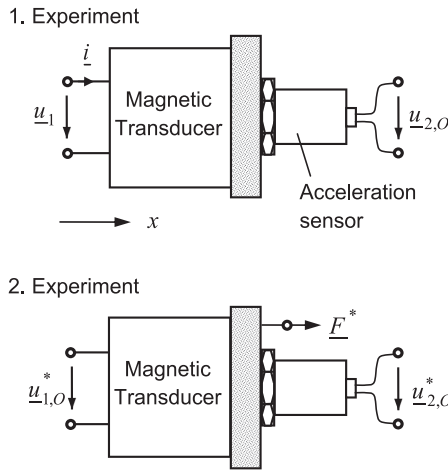


Figure 16. Acceleration sensor calibration experiments.

assumed. The input current \underline{i} can be transformed into a voltage \underline{u}_i by means of a known resistor R_0 . Thus, the transfer factor of the acceleration \underline{B}_a can be traced back through the application of the reciprocity relations to relations of the measured voltages, the mass m , and angular frequency ω

$$|\underline{B}_a| = \sqrt{\frac{|\underline{z}_L| u_{2,O} u_{2,O}^*}{\omega^2 \underline{i} \underline{u}_{1,O}^*}} = \sqrt{\frac{mR_0 u_{2,O} u_{2,O}^*}{\omega \underline{u}_i \underline{u}_{1,O}^*}} \quad (28)$$

Since these quantities can be measured simple, fast, and highly accurate, an efficient calibration method results (Lenk et al., 2010).

Application of the reciprocity relationship for the calibration of measurement microphones

A currently indispensable application of reciprocity is the primary calibration of laboratory standard microphones. This is carried out by the national metrological institute (e.g. the Physikalisch Technische Bundesanstalt of Germany) to represent the unit of sound pressure Pascal (Pa). The unit is passed from these primary-calibrated standard microphones in turn to all to be calibrated microphones of the country by means of a comparative method.

The microphone calibration by the reciprocity method—described in its principles by MacLean (1940)—is currently the method by which the lowest measurement uncertainties can be obtained. There are two main reasons:

1. The first sound pressure measurement is based on the measurement of mechanical and electrical quantities which is possible with very high accuracy.

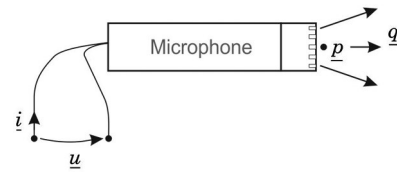


Figure 17. Electric and acoustic parameters on electrostatic measurement microphone.

2. The transfer function of measuring microphones depends on the acoustic boundary conditions under which the microphone is used.

Only with the help of the reciprocity procedure, the direct calibration for the metrological relevant cases—pressure chamber (DIN EN 61094-2:2009, 2009), free field (DIN EN 61094-3:1995, 1995), and diffuse sound field (Vorländer, 1996)—is currently possible.

The basis for the calibration is the reciprocity of electrostatic measurement microphones. As a prerequisite, they need to be operated in their sufficiently linear region. Figure 17 shows the definition of the electric and acoustic quantities for the electroacoustic two-port “microphone.” These are voltage u and current i at the electrical port as well as sound pressure p —averaged over the membrane surface—and acoustic volume flow, generated by the entire membrane, at the acoustic port. With these quantities, the electroacoustic circuit of the microphone in Figure 18 for the linear region can be specified. As the impedance matrix of the two-port network follows

$$\begin{pmatrix} \underline{u} \\ \underline{p} \end{pmatrix} = \begin{pmatrix} \underline{Z}_{eB} & -\underline{M} \cdot \underline{Z}_{aO} \\ \underline{M} \cdot \underline{Z}_{aO} & -\underline{Z}_{aO} \end{pmatrix} \cdot \begin{pmatrix} \underline{i} \\ \underline{q} \end{pmatrix} \quad (29)$$

where \underline{Z}_{eB} is the electrical impedance, generated when the acting total volume flow \underline{q} is 0. \underline{Z}_{aO} is the acoustic impedance for an electrical open port, that is, current \underline{i} is equal to 0. The transmission coefficient \underline{M} expresses both the ratio of the open-circuit voltage (current $\underline{i} = 0$) to the exciting pressure in the case of reception and the ratio of the short-circuit current volume flow (sound pressure $\underline{p} = 0$) to the applied current in the case of transmission to

$$\underline{M} = \underbrace{\frac{\underline{u}}{\underline{p}}}_{\text{Reception}} \Big|_{\underline{i}=0} = \underbrace{\frac{\underline{q}}{\underline{i}}}_{\text{Transmission}} \Big|_{\underline{p}=0} \quad (30)$$

For the calibration, one microphone is used as a transmitter and one microphone as a receiver (hereinafter distinguished by subscripts 1 and 2), as shown in Figure 19. The acoustic transmission path between the sound flow \underline{q}_1 generated by the transmitting microphone M1 and the sound pressure \underline{p}_2 at the reception microphone M2 is described by the impedance matrix

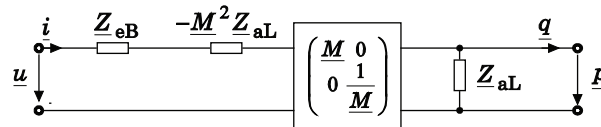


Figure 18. Electro-acoustic circuit of the microphone.

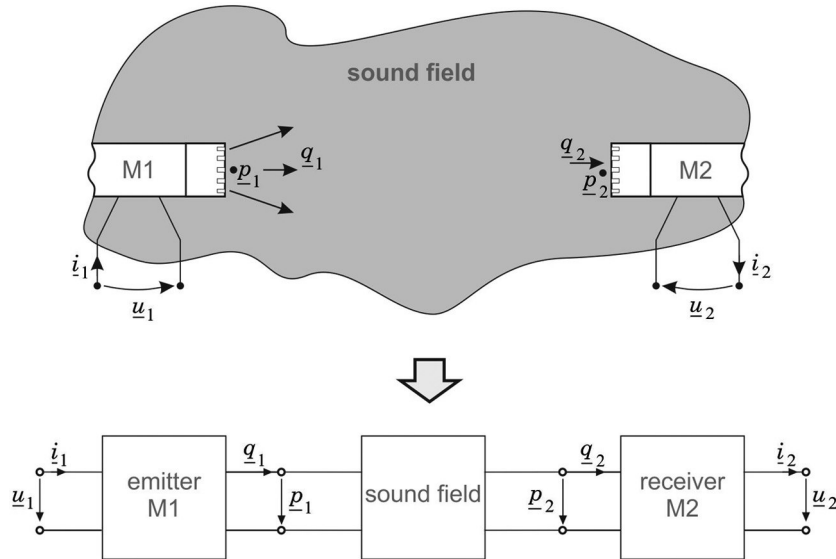


Figure 19. Microphone calibration setup.

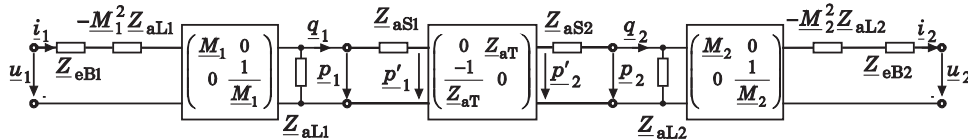


Figure 20. Equivalent circuit of the calibrator.

$$\begin{pmatrix} p_1 \\ p_2 \end{pmatrix} = \begin{pmatrix} Z_{aS1} & -Z_{aT} \\ Z_{aT} & -Z_{aS2} \end{pmatrix} \cdot \begin{pmatrix} q_1 \\ q_2 \end{pmatrix} \quad (31)$$

Figure 20 shows the resulting circuit of the entire calibration system.

Different acoustic impedance matrices result, depending on whether the calibration takes place in the pressure chamber, in the free field, or diffuse sound field. Subsequently, the next steps illustrate free-field calibration. For the free-field calibration according to DIN EN 61094-3:1995 (1995), the free-field transfer function

$$\underline{M}_f = \left. \frac{u}{p} \right|_{i=0} = \left. \frac{q}{i} \right|_{p'=0} \quad (32)$$

is introduced with respect to the sound pressure p' , which would act as applied sound at an non-movable

microphone diaphragm ($q = 0$) and where the prime sign denotes only that it is the pressure directly at the two-port core. Thus, the effect of acoustic radiation impedances Z_{aS1} and Z_{aS2} is already taken into account in the transfer functions \underline{M}_{f1} and \underline{M}_{f2} . The transmission path between the microphones simplifies to

$$\begin{pmatrix} p'_1 \\ p'_2 \end{pmatrix} = \begin{pmatrix} 0 & -Z_{aT} \\ Z_{aT} & 0 \end{pmatrix} \cdot \begin{pmatrix} q_1 \\ q_2 \end{pmatrix} \quad (33)$$

with the acoustic transfer impedance

$$Z_{aT} = \frac{j\omega\rho}{4\pi d_{12}} \cdot e^{-2d_{12}} \quad (34)$$

which describes the propagation of sound in a free field. Here, ρ is the density of the air, c the speed of sound, γ the complex propagation coefficient, and d_{12} the

distance between the acoustic centers of the microphones. For the free-field calibration, the electrical transfer impedance follows

$$\underline{Z}_{e12} = \frac{u_2}{i_1} = \underline{M}_{f1} \cdot \underline{Z}_{aT} \cdot \underline{M}_{f2} \quad (35)$$

Together with the known acoustic transfer impedance \underline{Z}_{aT} , one obtains the product of two transfer coefficients by the measurement of i_1 and u_2 . Because of reciprocity $\underline{Z}_{e12} = \underline{Z}_{e21}$, the swapping of transmitter and receiver provides no additional information. However, since the transfer function of a transmission path from two microphones is not of interest, but the transfer function of each microphone, it is necessary to add a third microphone and to measure the microphones in pairs. This yields three equations from which the three desired transfer coefficients

$$\begin{aligned} \underline{M}_{f1} &= \sqrt{\frac{1}{\underline{Z}_{aT}} \frac{\underline{Z}_{e12} \cdot \underline{Z}_{e13}}{\underline{Z}_{e23}}} \\ \underline{M}_{f2} &= \sqrt{\frac{1}{\underline{Z}_{aT}} \frac{\underline{Z}_{e23} \cdot \underline{Z}_{e12}}{\underline{Z}_{e13}}} \\ \underline{M}_{f3} &= \sqrt{\frac{1}{\underline{Z}_{aT}} \frac{\underline{Z}_{e13} \cdot \underline{Z}_{e23}}{\underline{Z}_{e12}}} \end{aligned} \quad (36)$$

of the microphones can be calculated.

In summary, only measurements of voltage, current, and effective distance as well as knowledge of frequency, air density, and sound velocity were necessary for the determination of the microphone transfer functions. Using reciprocity calibration, extremely low measurement uncertainties for acoustics of ≤ 0.05 dB are reached in the frequency range of 31.5 Hz to 8 kHz (free-field and pressure chamber calibration; Bork et al., 2007). Even in the lower ultrasonic range of 20–160 kHz, measurement uncertainties of less than 0.2 dB were achieved (Bouaoua, 2008) for the free-field calibration of 1/4" microphones. There is currently no alternative method which achieves a similar low measurement uncertainty and which is suited for the calibration in the pressure chamber, in the free field, and in the diffuse sound field.

As a future supplement to reciprocity, the use of optical measurement methods for the calibration of microphones is subject of this research (see Koukoulas et al., 2008; Theobald et al., 2002). These methods have not yet achieved the lowest measurement uncertainties of reciprocity.

Application of the reciprocity relations for linearity check of systems

Since linearity is one prerequisite of reciprocity, an obvious way to perform a check on linearity of a

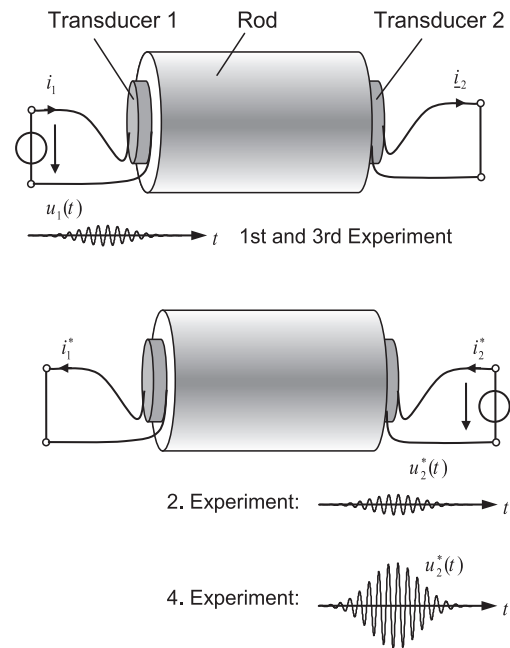


Figure 21. Coupling of two piezoelectric transducers with a rod.

system results in utilizing reciprocity relations. A structure is analyzed metrologically in a way whether the component arrangement fulfills the reciprocity relation. At sufficiently small signals, one expects consistent reciprocal relationships if the system behaves linearly. A fast subsequent performance of the two experiments eliminates cross sensitivities and parameter drifts most widely. If for larger signal magnitudes an increasingly growing deviation is found, it is ultimately due to nonlinearities in the system. Here, the source of nonlinearity and its strength cannot be initially identified. This method allows a check for sufficient linearity using a configuration in which only one branch with respect to its linearity is unknown. Since under correct boundary conditions the reciprocity yields to identical signal forms, the check of the linearity can be traced back to a time measurement.

The method is demonstrated exemplarily by the coupling of two piezoelectric transducers by a rod, as depicted in Figure 21. It is assumed that the rod shows sufficient linear behavior. In a first experiment, transducer 1 is excited with a low-voltage magnitude, which is in the linear region of the transducer. At transducer 2, a transient short-circuit current signal is measured. By the evaluation of the transmitted voltage and the received current signal, the transit time $t_{1,1}$ between the electrical ports of the electromechanical system can be determined based on the signal form. If transducer 2 is excited in the second experiment with a low-voltage magnitude and transducer 1 is used as a receiver, the measured transit time is $t_{1,2} = t_{1,1}$ as consequence of the reciprocity since both measured signals do not differ. There is no time difference Δt between the measuring directions.

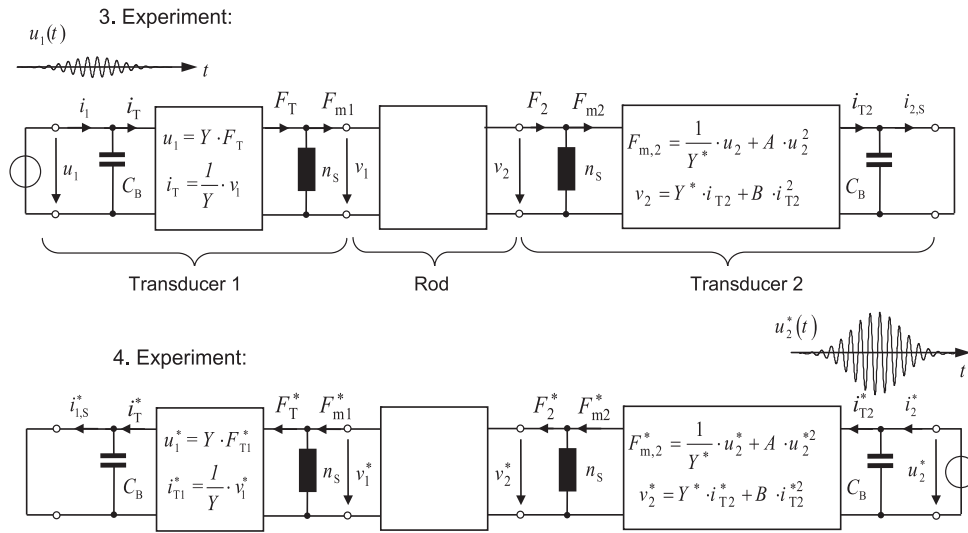


Figure 22. Equivalent circuit of the coupled piezoelectric transducers due to the amplitude-depending time delay difference the nonlinearity can be assigned to coefficient A .

Then, the third and the fourth experiments are performed subsequently. The third experiment is identical to the first experiment. In the fourth experiment, the excitation voltage magnitude at transducer 2 is increased. Therefore, transducer 2 leaves the linear operation range and the prerequisite for the reciprocity is violated. This, in turn, leads to a change in the transit time $t_{2,2}$. Compared to the transit time $t_{2,1}$ in the opposite direction with the low excitation voltage at transducer 1, a time difference $\Delta t = t_{2,2} - t_{2,1} \neq 0$ results. This time difference can be used as a measure for the nonlinearity of transducer 2. The nonlinearity of transducer 1 can be studied in an additional experiment where the excitation voltage at transducer 2 is kept low and the excitation voltage at transducer 1 is raised.

The magnitude-dependent nonlinearity is modeled with an additional quadratic factor A in the transducer relation of the equivalent circuit in Figure 22. When the experiments are performed below the rod's first natural frequency, the rod can be modeled by a T-circuit consisting the rod's compliance and mass. The factor A is determined by simulation experiments using the equivalent circuit where the time delay difference is reproduced. The basic idea is to keep all parameters equal in both measurements, except one. When the measurements can be described this way, then the source of the nonlinearity is found. This way, the nonlinearity can be captured with little effort.

Summary

Reciprocal linear time-invariant systems are an essential basis in electromechanical metrology. The article shows some examples for calibration, reduction in measurement uncertainty, and checking of nonlinearities,

where reciprocal relations of time-invariant linear networks are utilized in different ways. This applies in particular for linear systems, which include continuously distributed media.

Acknowledgements

The authors would like to thank Prof. Albrecht Reibiger (Technische Universität Dresden) and the editorial reviewers who volunteered their time and expertise to read and critique the article and for their constructive comments.

Declaration of Conflicting Interests

The author(s) declared no potential conflicts of interest with respect to the research, authorship, and/or publication of this article.

Funding

The author(s) received no financial support for the research, authorship, and/or publication of this article.

References

- Bork I, Fedtke T and Ratschko D (2007) Kalibrierungen von Messmikrofonen—die Basis der Bestimmung akustischer Größen. *PTB Mitteilungen* 117(1): 7–13.
- Bouaoua N (2008) *Free-field reciprocity calibration of condenser microphones in the low ultrasonic frequency range*. PhD Thesis, University of Oldenburg, Oldenburg.
- Carpenter C (1968) Magnetic equivalent circuits. *Proceedings of the IEEE* 115: 1503–1511.
- Deskur J (1999) Models of magnetic circuits and their equivalent electrical diagrams. *COMPEL: The International Journal for Computation & Mathematics in Electrical & Electronic Engineering* 18: 600–610.
- Desoer CA and Kuh ES (1969) *Basic Circuit Theory*. New York: McGraw-Hill.

- DIN EN 61094-2:2009 (2009) Messmikrofone—Teil 2: primärverfahren zur Druckkammer-Kalibrierung von Laboratoriums-Normalmikrofonen nach der Reziprozitätsmethode (IEC 61094-2:2009); Deutsche Fassung EN 61094-2:2009.
- DIN EN 61094-3:1995 (1995) Messmikrofone—Teil 3: primärverfahren zur Freifeld-Kalibrierung von Laboratoriums-Normalmikrofonen nach der Reziprozitätsmethode (IEC 1094-3:1995); Deutsche Fassung EN 61094-3:1995.
- Gerlach G and Dötzel W (2008) *Introduction to Microsystem Technology*. Chichester: John Wiley & Sons.
- Kellogg RA, Flatau AB, Clark AE, et al. (2005) Quasi-static transduction characterization of Gallfenol. *Journal of Intelligent Material Systems and Structures* 16: 471–476.
- Koenig HE, Tokad Y and Kesavan HK (1967) *Analysis of Discrete Physical Systems*. New York: McGraw-Hill.
- Koukoulas T, Theobald P, Schlicke T, et al. (2008) Towards a future primary method for microphone calibration: optical measurement of acoustic velocity in low seeding conditions. *Optics and Lasers in Engineering* 46(11): 791–796.
- Kuh ES and Rohrer RA (1967) *Theory of Linear Active Networks*. San Francisco, CA: Holden-Day, Inc.
- Lenk A, Ballas RG, Werthschützky R, et al. (2010) *Electromechanical Systems in Microtechnology and Mechatronics*. Heidelberg; New York: Springer.
- MacLean WR (1940) Absolute measurement of sound without a primary standard. *Journal of the Acoustical Society of America* 12(1): 140–146.
- Marschner U, Datta S, Starke E, et al. (2014a) Equivalent circuit of a piezomagnetic unimorph incorporating single-crystal gallfenol. *IEEE Transactions on Magnetics* 50(11): 8002504.
- Marschner U, Gerlach G, Starke E, et al. (2014b) Equivalent circuit models of two-layer flexure beams with excitation by temperature, humidity, pressure, piezoelectric or piezomagnetic interactions. *Journal of Sensors and Sensor Systems* 3: 187–211.
- Marschner U, Starke E, Adolphi B, et al. (2008) Transducer models of a magnetostrictive gallfenol sensor with solenoid or planar coil. In: *Proceedings of the Eurosensors XXII*, Dresden, 7–10 September 2008, pp. 93–96. Düsseldorf: VDI (on CD-ROM, ISBN 978-3-00-025217-4).
- Marschner U, Starke E and Pfeifer G (2013) Efficient dynamic modeling and simulation of smart structures with (equivalent) circuits. In: *Proceedings of the ASME 2013 conference on smart materials, adaptive structures and intelligent systems*, paper no. SMASIS2013-3260, vol. 1, pp. V001T03A040. New York: ASME.
- Reibiger A (2011) Foundations of network theory. *COMPEL: The International Journal for Computation & Mathematics in Electrical & Electronic Engineering* 30(4): 1319–1332.
- Reinschke K and Schwarz P (1976) *Verfahren zur rechnergestützten Analyse linearer Netzwerke*. Berlin: Akademie-Verlag.
- Schottky W (1926) Das Gesetz des Tiefenempfangs in der Akustik und Elektroakustik. *Zeitschrift für Physik* 36: 689–736.
- Theobald P, Preston R, Robinson S, et al. (2002) *Fundamental Standards for Acoustics Based on Optical Methods: First Stage Report*. Teddington: National Physical Laboratory.
- Vorländer M (1996) *Maximalfolgen-Reziprozitätskalibrierung von Mikrofonen im Halbraum*. Dresden: Habilitationsschrift TU Dresden.